Segmentation and Separation of Venous Vasculatures in Liver CT Images

Lei Wang, Christian Hansen, Stephan Zidowitz, Horst K. Hahn

Fraunhofer MEVIS - Institute for Medical Image Computing, Bremen, Germany

ABSTRACT

Computer-aided analysis of venous vasculatures including hepatic veins and portal veins is important in liver surgery planning. The analysis normally consists of two important pre-processing tasks: segmenting both vasculatures and separating them from each other by assigning different labels. During the acquisition of multi-phase CT images, both of the venous vessels are enhanced by injected contrast agent and acquired either in a common phase or in two individual phases. The enhanced signals established by contrast agent are often not stably acquired due to non-optimal acquisition time. Inadequate contrast and the presence of large lesions in oncological patients, make the segmentation task quite challenging. To overcome these difficulties, we propose a framework with minimal user interactions to analyze venous vasculatures in multi-phase CT images. Firstly, presented vasculatures are automatically segmented adopting an efficient multi-scale Hessian-based vesselness filter. The initially segmented vessel trees are then converted to a graph representation, on which a series of graph filters are applied in post-processing steps to rule out irrelevant structures. Eventually, we develop a semi-automatic workflow to refine the segmentation in the areas of inferior vena cava and entrance of portal veins, and to simultaneously separate hepatic veins from portal veins. Segmentation quality was evaluated with intensive tests enclosing 60 CT images from both healthy liver donors and oncological patients. To quantitatively measure the similarities between segmented and reference vessel trees, we propose three additional metrics: skeleton distance, branch coverage, and boundary surface distance, which are dedicated to quantifying the misalignment induced by both branching patterns and radii of two vessel trees.

Keywords: liver surgery planning, vascular segmentation, computer-assisted surgery

1. INTRODUCTION

Liver venous vasculatures include hepatic veins (HV) and portal veins (PV), which can be enhanced by contrast agents administrated in multi-phase computer tomography (CT) images of livers. In liver surgery planning, the analysis of venous vascular structures in livers is required to explore patient-individual branching patterns. Segmentation and separation of liver vasculatures serve as two fundamental steps in the tools of computer-assisted surgery planning. Combined with tumor segmentation, spatial relations between vessels and tumors can be quantitatively analyzed. Moreover, the segmentation of vessels builds the basis for vascular risk analyses[1] and virtual resection planning.[2] However, the complexity of vasculature and the low contrast between vessels and surrounding tissues due to imperfect contrast enhancement make these tasks challenging. In this work, we present a dedicated framework to segment and separate hepatic veins and portal veins for liver surgery planning in multi-phase CT images. Additionally, three metrics, including skeleton distance, branch coverage and boundary surface distance, are defined to quantitatively and objectively assess the misalignment between segmented and reference vessels.

2. METHODS

The proposed framework consists of two major steps: the segmentation and interactive separation of HV and PV. In multi-phase liver CT, contrast enhanced images of HV and PV can be either acquired in a common phase or two individual phases. The proposed method is capable of handling both cases to segment HV and PV simultaneously or individually. Figure 1 illustrates the processing pipeline.

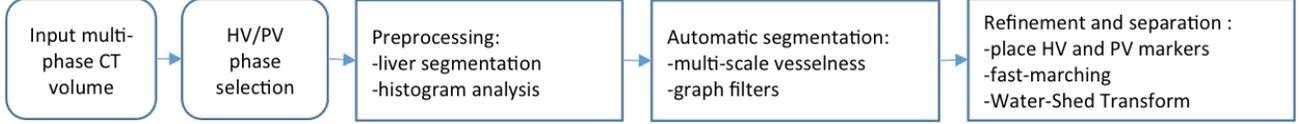| Input multi-phase CT volume	→	HV/PV phase selection	→	Preprocessing: -liver segmentation -histogram analysis	→	Automatic segmentation: -multi-scale vesselness -graph filters	→	Refinement and separation : -place HV and PV markers -fast-marching -Water-Shed Transform

Figure 1. Schematic overview of the work flow.

2.1 Preprocessing

In preprocessing, we segment the liver on the selected venous phase (see Fig 2(a)). The liver mask confines the calculation of vesselness response within the liver to reduce computational expense. Due to the enhancement by contrast agent, venous structures appear as hyperdense. To preclude the extreme hypodense voxels that definitely don't belong to HV and PV, we analyze the histogram of the liver CT image and determine a minimum threshold L_{min}, corresponding to the peak of the histogram distribution. We assume that the venous voxels should not appear with the highest frequency in the liver, which means that any voxels below L_{min} are assumed not belonging to venous vessels and will be excluded from subsequent steps.

2.2 Automatic initial segmentation of HV and PV

Hessian-based filters have been widely employed to enhance tube-like structures in 3D images. There are several vesselness filters published in previous works.[3,4] Because the contrast of venous vessels in different input images are quite heterogeneous, we choose the multi-scale, Hessian-based vesselness filter introduced by Frangi et al. to enhance the vessels in a CT volume.[3] The major benefits of Frangi's vesselness filter include the integration of information from all three Eigenvalues and the independence from their absolute values, which are associated with contrast levels of vessels. The outputs of the filter are scaled within the range between 0 and 1. Assuming the Eigenvalues of Hessian matrix are sorted in order: $|\lambda_1| \leq |\lambda_2| \leq |\lambda_3|$, Frangi's vesselness filter is defined as following:

$$f(\sigma) = \begin{cases} 0 & \text{if} \quad \lambda_2 > 0 \ \text{or} \ \lambda_3 > 0 \\ \left(1 - \exp\left(\frac{-R_A^2}{2\alpha^2}\right)\right) \exp\left(\frac{-R_B^2}{2\beta^2}\right) \left(1 - \exp\left(\frac{-S^2}{2c^2}\right)\right) & \text{otherwise} \end{cases} \tag{1}$$

where
$$R_A = |\lambda_2|/|\lambda_3|, \qquad R_B = \frac{|\lambda_1|}{\sqrt{|\lambda_2 \lambda_3|}}$$
and
$$S = \sqrt{\lambda_1^2 + \lambda_2^2 + \lambda_3^2}.$$

The ratio R_A is designed to differentiate vessels from sheet-like structures, whereas R_B is used to distinguish vessels from blob-like structures. The term S aims to suppress noise structures. The scale parameter σ indicates the size of Gaussian kernel used for calculating Hessian matrix. The parameters used in this filter, α, β and c are set to $0.5, 0.5$ and 10. Considering the radius range of HV and PV, we choose three optimized scales for σ: 1.5 mm, 2.25 mm, and 3 mm based on our experimental tests, which are able to capture vessels with thin, medium, and thick radii (see Fig. 2(b)). The ultimate vesselness response is obtained by extracting the maximum across all scales. Normally, calculating the Hessian matrix is quite expensive when increasing the size of Gaussian kernel. To speed up, we adopt an inverse multi-scale strategy which keeps the kernel size constant at 1.5 mm, but downsamples input volumes to larger voxel spacing.

On the basis of vesselness response, we initially segment HV and PV utilizing an automatic region-growing algorithm. The seeds of region-growing are automatically found by analyzing the histogram of vesselness outputs. All voxels with a vesselness value between 90_{th} and 99_{th} percentiles are taken as seed points. The lower and upper thresholds of region growing are chosen as 75_{th} and 99.9 percentiles, respectively. If the HV and PV possess high contrast against their surrounding structures, the initial segmentation normally yields satisfactory results (see Fig. 2(c)).

2.3 Refinement of HV and PV segmentations

In case the HV and PV exhibit extremely low contrast, or large hypodense lesions with internal hyperdense structures are present, many irrelevant structures will be enhanced as well by the vesselness filter and captured in the region-growing step. For refinement, we first transform the segmented vessel trees into a graph representation[5] and validate the graph tree using two graph filters. Unconnected components of the segmented vessels will be transformed into different graph trees. Each graph tree has three basic elements: root, node, and edge. One of the attributes of a graph tree is volume size. The first filter introduces a lower limit to the volume size of each individual graph tree. The graph trees with volume less than 0.5 ml are filtered out. Hence, unconnected components can be removed by this filter. Additionally, we measure the edge length of all branches in a graph tree and assign a minimum threshold to truncate small branches shorter than 10 mm. From our experiments, these two graph filters are able to rule out isolated trees and prune spurious branches (see Fig. 2(d)).

Other issues lie in the areas of inferior vena cava and entrance of PV, which are normally not enclosed by the liver mask and thus not segmented. Moreover, the inferior vena cava can be hypodense or hyperdense depending on the density of contrast agent. We propose a robust interactive solution to recover the segmentation in both regions. Two markers need to be placed in the regions of inferior vena cava and entrance of PV (see Fig. 2(e)). Then, a fast marching algorithm is applied in the predefined neighborhoods of these two markers.[6] The speed map of fast marching is determined by commonly used Sigmoid filter which applies Sigmoid function on intensities.[7] A local spherical neighborhood region with a radius of 20 mm is defined for each marker. The parameters α_{sig} and β_{sig} of the Sigmoid function are set as 10 and the mean intensity of the voxels in defined spherical neighborhoods, respectively. The stop value of propagation is set to 50. The efficient computation of the algorithm permits instant display of the segmented region when each marker is adjusted, until the optimal position is reached.

2.4 Separation of HV and PV

The HV and PV will be simultaneously segmented when they present in a common phase. For liver surgical planning, it is demanding to separate and analyze them individually. The separation process is triggered when HV and PV markers are placed. To meet time constraints, we employ an interactive watershed transform algorithm that takes the HV and PV markers as the seed points of two different classes.[8] The cost image of the watershed transform is the original intensity image, smoothed with an edge-preserving diffusion filter. The entire volume is classified into two classes associated with the HV and PV markers. Eventually, the segmented HV and PV can be separated by applying the class labels on the segmentation results (see Fig. 2(f)).

3. RESULTS

3.1 Dataset

To evaluate the performance of the proposed method, a test set enclosing 60 multi-phase hepatic CT scans acquired from 30 liver donors and 30 oncological patients was collected. HV/PV phases were taken for all scans. The volumes of HV/PV were manually segmented by an experienced radiologist, serving as reference for quantitative evaluation. In addition, the markers used to refine and separate the HV and PV were placed manually and saved prior to automatic testing. Image resolution of HV/PV phases in test images ranges from $512 \times 512 \times 189$ to $512 \times 512 \times 310$. Calculation of the multi-scale vesselness filter takes 15 to 40 seconds depending on different image resolutions. The initial segmentation and subsequent refinement of HV/PV take maximally 3 seconds using a 3.07 GHz Intel CPU.

3.2 Evaluation metrics

Evaluating the alignment of two vessel trees is not as easy as other mass objects. Two major features characterizing a tree structure are branching patterns and radii. To measure the consistency of branching patterns and radii more specifically, besides the widely used overlap metric: Dice Coefficient (DC), we introduce three additional metrics: skeleton distance, branch coverage, and boundary surface distance. First of all, the skeletons (indicated as SK_{seg} and SK_{ref}) of the segmented and reference vessel volumes (indicated as V_{seg} and V_{ref}) are extracted, and similarly the boundary surfaces (indicated as BS_{seg} and BS_{ref}) of both volumes are automatically derived as well.
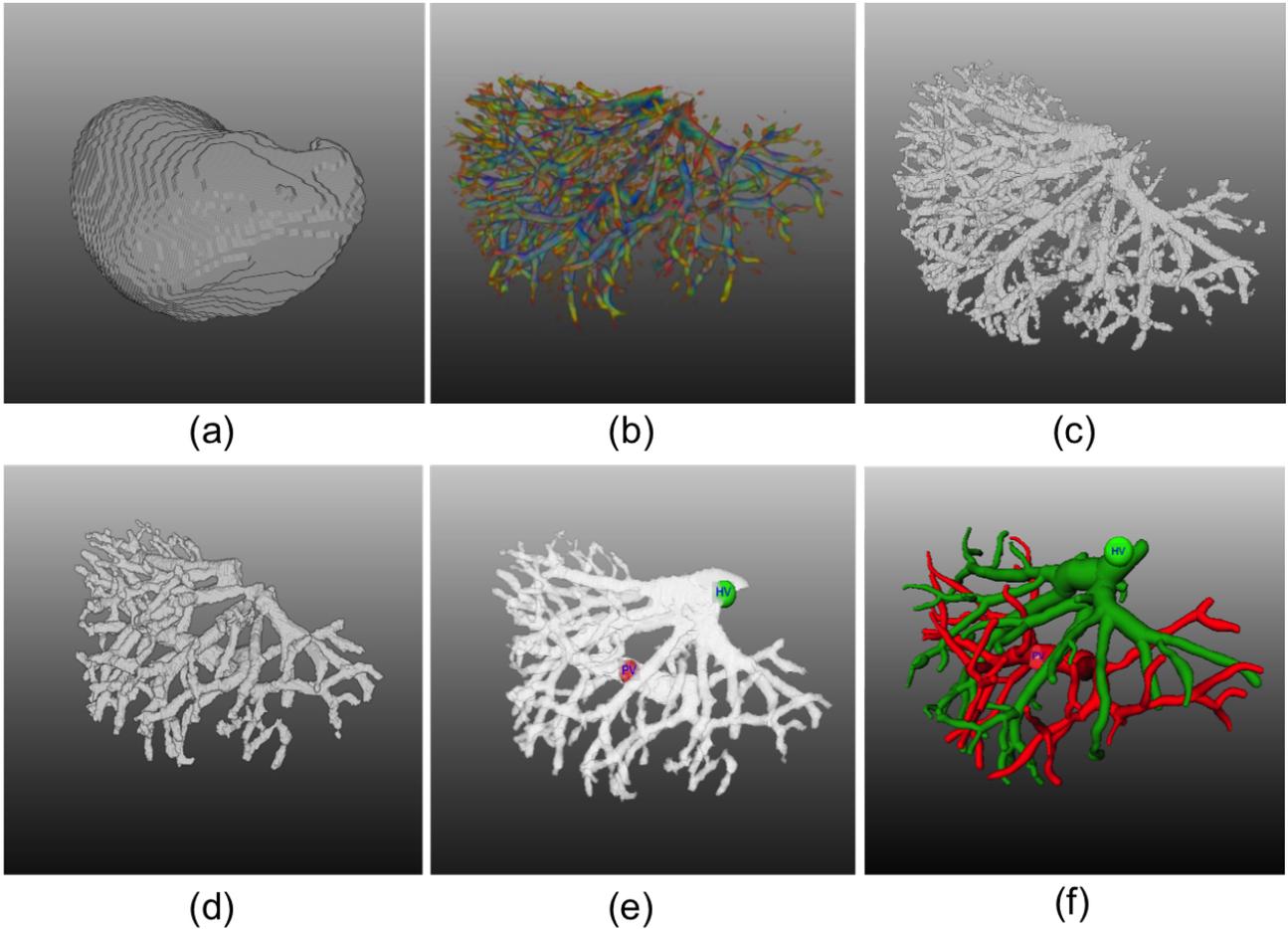
Figure 2. HV/PV segmentation and separation: (a) segmented liver mask; (b) response of multi-scale vesselness filter represented with color map: red, green and blue indicates response of small, medium and large scales, respectively; (c) initial segmentation of HV/PV; (d) HV/PV segmentation after graph filters; (e) interactive refinement of HV/PV segmentation: HV and PV markers displayed with green and red dots; (f) result of separating HV and PV.
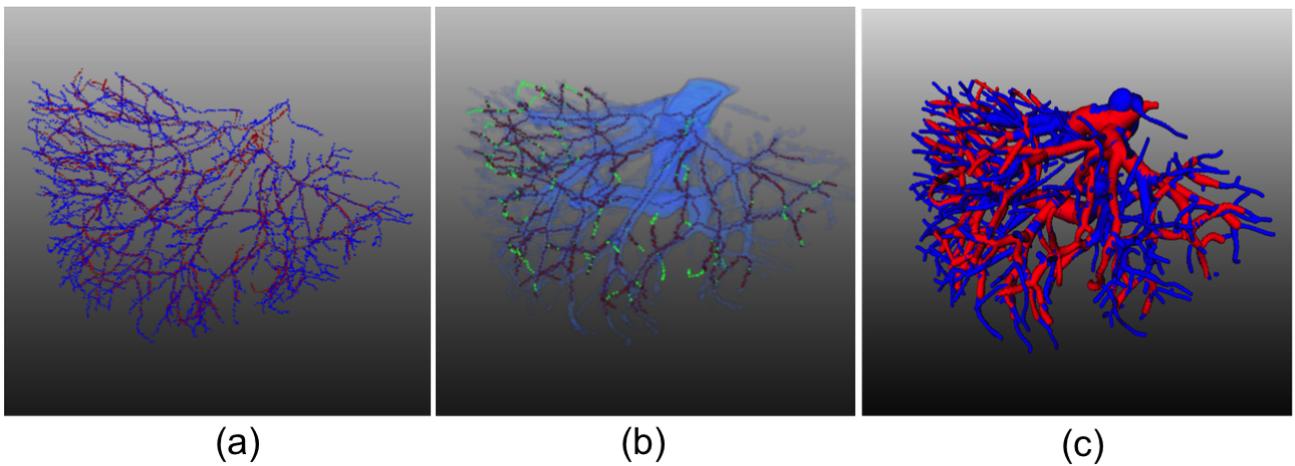

Figure 3. Depiction of evaluation metrics: (a) computation of distance between reference skeleton (blue) and segmented skeleton (red); (b) calculating proportion of segmented skeleton (red) covered by reference volume (light blue), and the uncovered skeletons are indicated in green; (c) surface distance between segmented volume (red) and reference volume (blue).

3.2.1 Dice Coefficient

Dice Coefficient (DC) is computed to measure the overlap between V_{seg} and V_{ref}. Generally, it is able to reflect both misalignment of branches and errors of radii to some extent. The results obtained for the calculation of DC were 0.52 ± 0.11 ($mean \pm stdev$)

3.2.2 Skeleton distance

Skeleton distance metric aims to particularly measure the alignment of branching patterns by computing the distance between two skeletons: SK_{seg} and SK_{ref} (see Fig. 3(a)). It is a bi-directional distance measure. The average distance from SK_{seg} to SK_{ref} is calculated as following: for each point of SK_{seg}, its paired point on SK_{ref} was defined as the one with the least distance to it. The sum distance was computed over all these point pairs. Ultimately, the average distance $D_{seg2ref}$ was calculated by dividing the sum distance with the count of point pairs. Inversely, the average distance $D_{ref2seg}$ from SK_{ref} to SK_{seg} can be obtained in the same way. Ultimately, the average distance between SK_{seg} and SK_{ref} is defined as $D = (D_{seg2ref} + D_{ref2seg})/2$. Experiments showed that the mean of D was 7.82 mm with a standard deviation of 2.96 mm. In Fig. 4, the distributions of Dice Coefficient and skeleton distance illustrated by box-and-whisker plots were given.

3.2.3 Branch coverage

Branch coverage metric $P_{seg2ref}$ reports the percentage of SK_{seg} covered by the corresponding reference volume V_{ref} (see Fig. 3(b)), and the same percentage $P_{ref2seg}$ is computed inversely for the skeleton of reference SK_{ref}. The average P of the two percentages depicts branching consistency of both vessel trees from another perspective. More specifically, it is able to reflect two typical types of errors arose in segmentation problems: under-segmentation or over-segmentation. Under-segmentation correlates with the relation that $P_{seg2ref}$ is greatly larger than $P_{ref2seg}$, and over-segmentation behaves in opposite way. The experimental results of the average branch coverage P achieved a mean of 0.64 with a standard deviation of 0.11.

3.2.4 Boundary surface distance

The metric of boundary surface distance investigates the deviation of both branching patterns and radii. It evaluates the distance between BS_{seg} and BS_{ref} (see Fig. 3(c)). Similar to the computation of skeleton distance, it is again a bi-directional distance. The distance from BS_{seg} to BS_{ref} is indicated as $SD_{seg2ref}$, and $SD_{ref2seg}$ represents the inverse distance. The average surface distance SD is derived by $SD = (SD_{seg2ref} + SD_{ref2seg})/2$. The mean and standard deviation of SD were 4.74 mm and 2.16 mm, respectively. Additionally, to fetch an overview of the distributions of branch coverage and surface distance, the box plots of these two measures were demonstrated in Fig. 5.

3.2.5 Statistics of metrics

Table 1 lists the statistical results of all proposed metrics for the entire test cases. It is easy to observe that branch coverage from segmentation to reference is better than inverse direction on average. The reason is that our radiologists tends to delineate the complete reference vessels including very thin vasculatures whose radii are less than 1 mm, which are normally not detected by the method and of less interest for liver surgical planning in clinical practice.

To better correlate visual inspection with the proposed quantitative metrics, four exemplary segmented and corresponding reference masks of HV and PV are visualized in Fig. 6, where the values of associated metrics for each case were attached. Notice that branch coverage P manifests the same trend with Dice Coefficient. However, skeleton distance D and boundary surface distance SD behave slightly differently compared to DC in the first two cases, where case 2 has a larger DC, but larger distance errors expressed by D and SD. The reason is that they basically measure the distances in different dimensions. D tries to measure the distance between lines, and SD measures the distance between surfaces, whereas DC measures the distance between volumes. Therefore, they reflect the two types of errors, branching patterns and radii, with different strength and focus. Table 2 lists the focus of each metric in measuring misalignment of two vessel trees. In case 2, a larger DC value indicates a better alignment in the parts with larger volume sizes, such as vena cava, whereas its alignment with respect to branching patterns is actually worse than case 1 slightly, because a larger SD is observed. In this sense, SD is a more reliable metric than DC in reflecting both errors brought by branching patterns and radii in comparison of vessel trees.

Table 1. The statistical analysis results of the volumetric difference and surface distance measurements

	DC	$D_{seg2ref}$ (mm)	$D_{ref2seg}$ (mm)	D (mm)	$P_{seg2ref}$	$P_{ref2seg}$	P	$SD_{seg2ref}$ (mm)	$SD_{ref2seg}$ (mm)	SD (mm)
Mean	0.52	4.92	10.72	7.82	0.78	0.51	0.64	3.30	6.18	4.74
Stdev	0.11	5.29	3.26	2.96	0.19	0.13	0.11	3.97	2.18	2.16
Min	0.25	1.02	5.12	4.81	0.23	0.18	0.28	0.55	3.44	2.38
Max	0.68	30.70	24.15	20.37	0.99	0.77	0.79	23.37	14.31	14.11

Table 2. Metrics and if they express a specific type of misalignment error

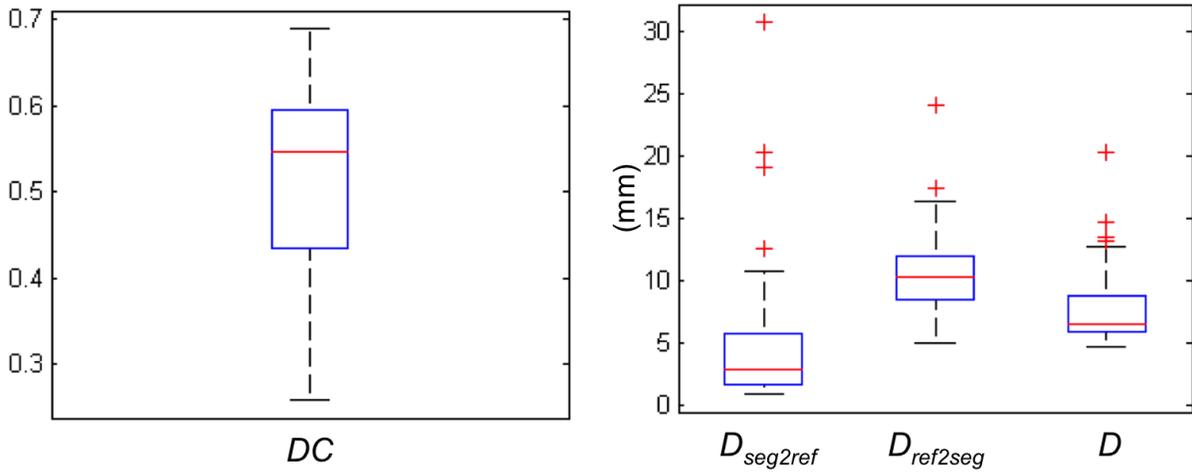|	Dice Coefficient DC	skeleton distance D	branch coverage P	surface distance SD
branching pattern errors	Yes	Yes	Yes	Yes
radii errors	Yes	No	No	Yes

Figure 4. Distribution of Dice coefficient and skeleton distance: box plot of DC (left); box plots of $D_{seg2ref}$, $D_{ref2seg}$ and D (right)
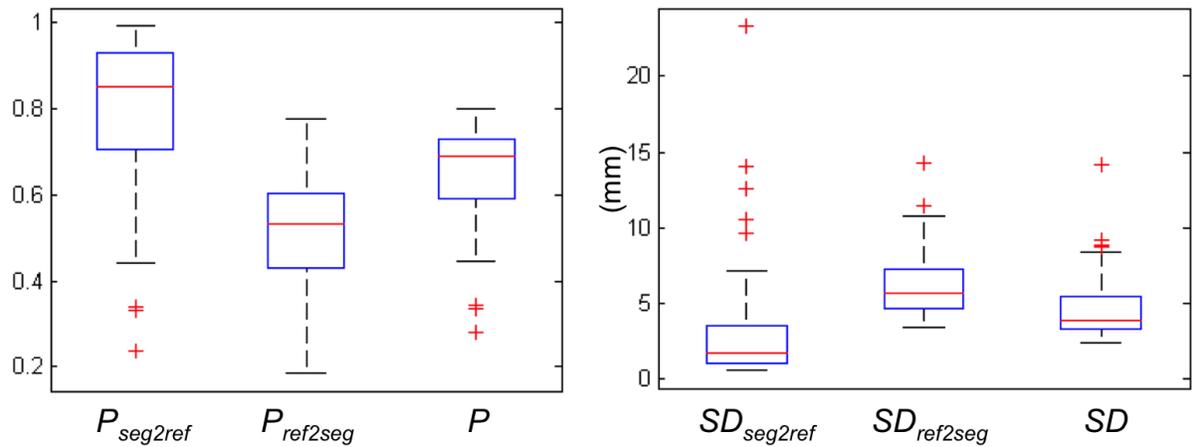

Figure 5. Distribution of brach coverage and boundary surface distance: box plots of $P_{seg2ref}$, $P_{ref2seg}$ and P (left); box plots of $SD_{seg2ref}$, $SD_{ref2seg}$ and SD (right)

Case 1:
DC = 0.65
$D_{seg2ref}$ = 1.55
$D_{ref2seg}$ = 8.14
D = 4.84
$P_{seg2ref}$ = 0.94
$P_{ref2seg}$ = 0.59
P = 0.77
$SD_{seg2ref}$ = 0.74
$SD_{ref2seg}$ = 4.02
SD = 2.38

Case 2:
DC = 0.68
$D_{seg2ref}$ = 1.48
$D_{ref2seg}$ = 8.74
D = 5.11
$P_{seg2ref}$ = 0.96
$P_{ref2seg}$ = 0.62
P = 0.79
$SD_{seg2ref}$ = 0.85
$SD_{ref2seg}$ = 4.52
SD = 2.68

Case 3:
DC = 0.38
$D_{seg2ref}$ = 7.60
$D_{ref2seg}$ = 10.93
D = 9.27
$P_{seg2ref}$ = 0.49
$P_{ref2seg}$ = 0.45
P = 0.47
$SD_{seg2ref}$ = 5.48
$SD_{ref2seg}$ = 6.66
SD = 6.07

Case 4:
DC = 0.44
$D_{seg2ref}$ = 3.18
$D_{ref2seg}$ = 9.26
D = 6.22
$P_{seg2ref}$ = 0.82
$P_{ref2seg}$ = 0.47
P = 0.65
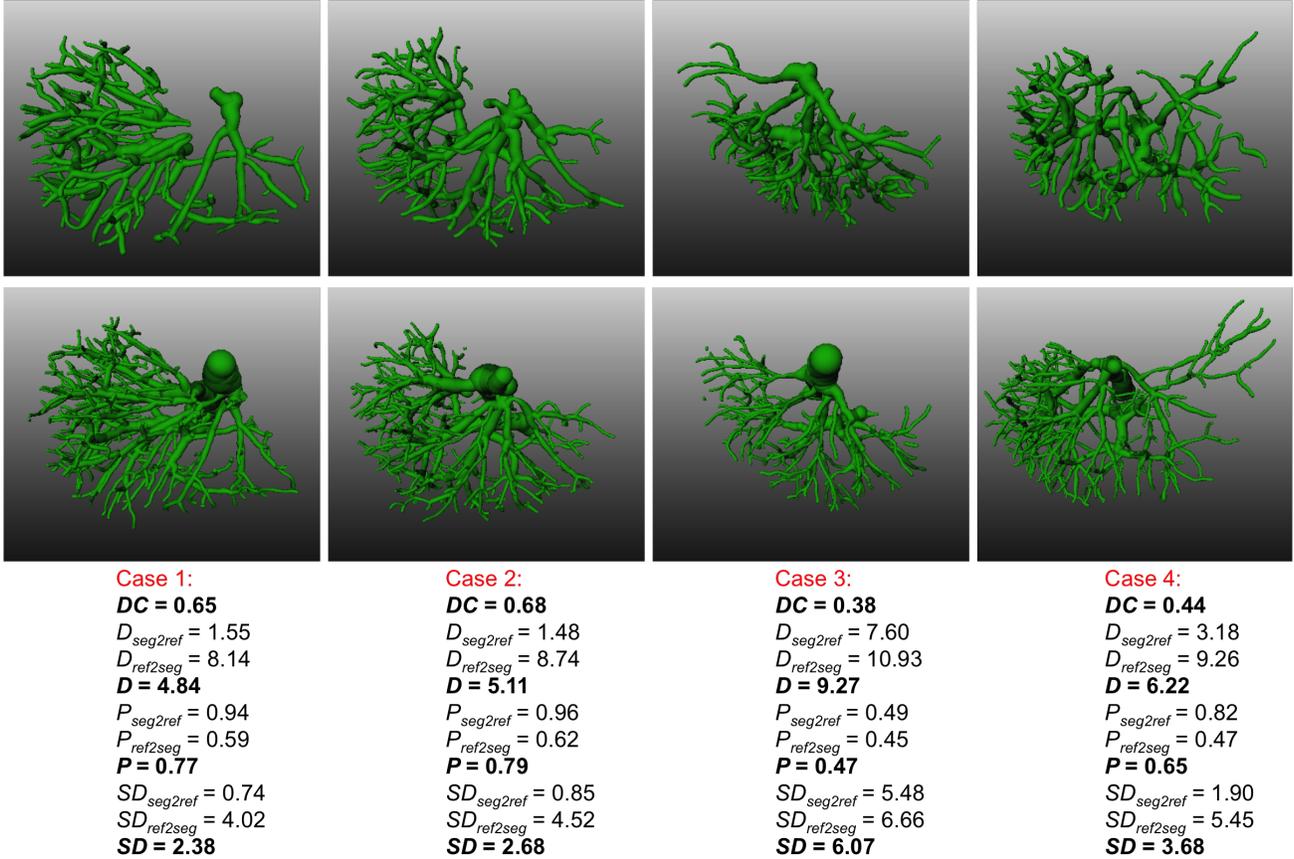$SD_{seg2ref}$ = 1.90
$SD_{ref2seg}$ = 5.45
SD = 3.68

Figure 6. Four examples of segmentation results and their associated metric values: segmented HV and PV (top row); reference segmentation of HV and PV (middle row); corresponding values of the metrics used for evaluation (bottom row). Each column relates with one particular case.

4. CONCLUSIONS AND DISCUSSIONS

In this work, we developed a semi-automatic approach which is dedicated to precisely segmenting and separating venous vasculatures in liver CT images, which is a crucial task for liver surgery planning. An extensive assessment for the proposed method was conducted with a large scale of test images, for which manual annotations by radiologists were built as the ground truth. Three new quantitative measurements: skeleton distance, branch coverage, and boundary surface distance, were proposed to review the performance from different perspectives.

Multi-scale vesselness filter is sensitive in detecting vascular structures in different contrast levels. Considering the balance between performance and computational expense, we choose three scales in this work, which consumes the time in acceptable range. In practice, the disturbing structures resembling vasculatures locally will be enhanced as well, especially in the patients with oncological lesions. The graph filters and manual editing tool in post-processing step are capable of ruling out these false positives. The optimal parameter settings for the graph filters used in post-processing were obtained through a brutal test iterating through all possible combinations. The success of Water-Shed transform algorithm used in separation of HV and PV depends on the marker positions. We search for the local maxima in the near of two placed seed markers and extend number of seeds by adding neighboring points. The correction of seed markers helps to improving the robustness and reliability of the separation method.

The proposed semi-automatic segmentation framework is capable of capturing venous vasculatures in both healthy and oncological livers. The latter cases normally consists of lesions with varied sizes and incomplete vasculatures. The extensive quantitative test proves the applicability in the application of computer-aided surgery planning. A user study, aiming to measure the performance gain, is planned for the further work.

REFERENCES

[1] Hansen, C., Zidowitz, S., Hindennach, M., Schenk, A., Hahn, H., and Peitgen, H. O., "Interactive determination of robust safety margins for oncologic liver surgery," *Int J Comput Assist Radiol Surg* **4**(5), 469–474 (2009).

[2] Konrad-verse, O., Preim, B., and Littmann, A., "Virtual Resection with a Deformable Cutting Plane," *In Proceedings of Simulation und Visualisierung* (1), 203–214 (2004).

[3] Frangi, A. F., Niessen, W. J., Vincken, K. L., and Viergever, M. A., "Multiscale vessel enhancement filtering," *Medical Image Computing and Computer-Assisted Intervention (MICCAI)* **1496**, 130–137 (1998).

[4] Descoteaux, M., Collins, D. L., and Siddiqi, K., "A geometric flow for segmenting vasculature in proton-density weighted MRI.," *Medical image analysis* **12**(4), 497–513 (2008).

[5] Selle, D., Preim, B., Schenk, A., and Peitgen, H.-O., "Analysis of vasculature for liver surgical planning.," *IEEE transactions on medical imaging* **21**(11), 1344–57 (2002).

[6] Sethian, J. A., "A fast marching level set method for monotonically advancing fronts," *Proceedings of the National Academy of Sciences* **93**(4), 1591–1595 (1996).

[7] Han, J. and Moraga, C., "The influence of the sigmoid function parameters on the speed of backpropagation learning," *From Natural to Artificial Neural Computation* **930**, 195–201 (1995).

[8] Hahn, H. and Peitgen, H., "The skull stripping problem in MRI solved by a single 3D watershed transform," *Medical Image Computing and Computer-Assisted Intervention (MICCAI)* **1935**, 134–143 (2000).